Appl Magn Reson
DOI 10.1007/s00723-017-0883-z

Applied Magnetic Resonance

ORIGINAL PAPER

Electron–Nuclear Spin Dynamics in Semiconductor QDs

M. S. Kuznetsova[1,2,3]

Received: 6 February 2017 / Revised: 12 April 2017

Abstract This work presents an overview of investigations of the nuclear spin dynamics in nanostructures with negatively charged InGaAs/GaAs quantum dots characterized by strong quadrupole splitting of nuclear spin sublevels. The main method of the investigations is the experimental measurements and the theoretical analysis of the photoluminescence polarization as a function of the transverse magnetic field (effect Hanle). The dependence of the Hanle curve profile on the temporal protocol of optical excitation is examined. Experimental data are analyzed using an original approach based on separate consideration of behavior of the longitudinal and transverse components of the nuclear polarization. The rise and decay times of each component of the nuclear polarization and their dependence on transverse magnetic field strength are determined. To study the role of the Knight field in the dynamic of nuclear polarization, a weak additional magnetic field parallel to the optical axis is used. We have found that, only taking into account the nuclear spin fluctuations, we can accurately describe the measured Hanle curves and evaluate the parameters of the electron–nuclear spin system in the studied quantum dots. A new effect of the resonant optical pumping of nuclear spin polarization in an ensemble of the singly charged (In,Ga)As/GaAs quantum dots subjected to a transverse magnetic field is discussed. Nuclear spin resonances for all isotopes in the quantum dots are detected in that way. In particular, transitions between the states split off from the $\pm 1/2$ doublets by the nuclear quadrupole interaction are identified.

✉ M. S. Kuznetsova
mskuznetsova85@gmail.com

[1] Physics Department, Saint Petersburg State University, 198504 St. Petersburg, Russia

[2] Spin Optics Laboratory, Saint Petersburg State University, 199034 St. Petersburg, Russia

[3] Experimentelle Physik 2, TechnischeUniversität Dortmund, 44221 Dortmund, Germany

Published online: 21 April 2017

1 Introduction

Spin dynamics in semiconductor quantum dots (QDs) has been an object of intense theoretical and experimental research during the past few decades [1–6]. In a QD, the spin of a confined electron is strongly coupled to the spins of lattice nuclei. The coupling strength is given by the contact hyperfine interaction, which is enhanced due to strong localization of the electron in the QD [2, 3]. The hyperfine coupling destroys electron spin polarization via interaction with random fluctuations of the effective nuclear magnetic field [2]. A way to overcome this effect is to create a strong polarization of the nuclear spins [3].

The dominant mechanism of the dynamic nuclear polarization (DNP) in semiconductors is the angular momentum transfer from optically oriented electrons to nuclei via electron–nuclear hyperfine interaction [7]. This process is particularly effective in quantum dot heterostructures, where the electron wave function covers a limited number of nuclei, and the electron and nuclear spins make up a strongly coupled system. Since the spin-polarized nuclei, in turn, create an effective magnetic field (the Overhauser field) which splits electron spin sublevels, the state of the nuclear spin system can be examined by the polarization-resolved spectroscopic methods. The methods based on studying the polarization of photoluminescence (PL) were extensively explored for study of nuclear spin dynamics in bulk semiconductors [7, 8]. Nuclear spin relaxation times were found to be a few seconds or longer [9]. Spectroscopic methods were widely used in the last two decades when the experimental technique was developed for study of PL spectra of single QDs [6, 10–12]. These experiments allowed one to detect strong effect of nuclear magnetic field and to perform the first experiments on detection of nuclear magnetic resonance of single QDs [13]. The measurements reported in recent years have also shown that nuclear spin relaxation in QDs is much faster. In particular, nuclear spin relaxation in a magnetic field applied parallel to the optical axis (the longitudinal magnetic field) was found to occur over times on the order of milliseconds [12, 14, 15].

An alternative approach for detection of nuclear polarization in QDs is to measure the electron polarization created by optical pumping in an external magnetic field. This method does not require high spectral resolution and can be applied to QD ensembles characterized by extremely broad lines in PL spectrum. As the nonequilibrium electron spin polarization depends on the total magnetic field, the Overhauser field can be detected using its effect on the mean electron spin, for example, observing the associated changes in the circular polarization of PL. In a longitudinal magnetic field, the nuclear polarization created by the pumping may affect the PL polarization by suppressing electron spin relaxation [14, 16, 17]. For optical pumping in a magnetic field perpendicular to the optical axis (the transverse magnetic field), the electron spin polarization is usually destroyed with increase of the magnetic field (the Hanle effect). In this case, the Overhauser field modifies the width and shape of the dependence of the circular polarization of the PL on the magnetic field (the Hanle curve), which can give rise to a nonmonotonous dependence, and even to a hysteresis [7, 8, 16, 18–24].

Here we discuss experimental study of the electron–nuclear spin dynamics in the singly charged (In,Ga)As/GaAs QDs in a transverse magnetic field under different

protocols of optical excitation. In particular, such experimental approach allows one to study the dynamics of the rise and decay of the nuclear spin polarization as it is discussed in Sect. 3, to highlight the role of nuclear spin fluctuations in the electron–nuclear spin dynamics (Sect. 4), and to study nuclear magnetic resonances [25] (Sect. 5).

2 Experimental Details [22, 26–28]

Heterostructures containing 20 layers of self-assembled (In,Ga)As/GaAs QDs separated by Si-δ-doped GaAs barriers were studied in the cited works. Donor ionization supplies every dot with, on average, a single resident electron. The original structure was grown by molecular-beam epitaxy on a (100) GaAs substrate. Then it was divided into several pieces which were then thermally annealed at different temperatures, $T_{\mathrm{ann}} = 900$ °C (sample A) and 980 °C (sample B) The annealing resulted in a reduction of the In content in the QDs due to interdiffusion of In and Ga atoms and in a high-energy shift of the lowest QD optical transition, $E_{\mathrm{A}} = 1.34$ eV, $E_{\mathrm{B}} = 1.42$ eV. The annealing also gave rise to a considerable decrease of mechanical stress in the QDs and, therefore, reduced the quadrupole splitting of nuclear spin states. Besides, the enlarging of localization volume for resident electrons occurred due to the interdiffusion of In and Ga atoms.

The studied samples were immersed in liquid helium at a temperature $T = 1.8$ K in a cryostat with a superconducting magnet. Magnetic fields up to 300 mT were applied perpendicular to the optical axis (Voigt geometry) along to the [110] crystallographic direction of the sample. To create an additional magnetic field, perpendicular to the main magnetic field and parallel to the optical axis, a pair of small Helmholtz coils was installed outside the cryostat.

The PL was excited by the circularly polarized light of a continuous wave (CW) Ti:sapphire laser, with the photon energy tuned to the optical transitions in the wetting layer of each sample ($E_{\mathrm{WL}} = 1.459$ eV for sample A and $E_{\mathrm{WL}} = 1.481$ eV for sample B). An electro-optical modulator followed by a quarter-wave plate is used to modulate the polarization helicity of optical excitation. The degree of circular polarization of the PL was typically detected by a standard method using a photoelastic modulator and an analyzer (a Glan–Taylor prism). The modulator creates a time-dependent phase difference, $\phi = (\pi/4)\sin(2\pi f \cdot t)$, between the linear components of the PL, thus converting each of the circular components ($\sigma+$ and $\sigma-$) into linear ones (x and y) at the modulation frequency, typically $f = 50$ kHz. The analyzer selects one of the linear components, which was dispersed with a 0.5-m monochromator and detected by an avalanche photodiode. The signal from the photodiode was accumulated for each circular PL component separately in a two-channel photon-counting system. The PL polarization was calculated using a standard definition, $\rho = (I^{++} - I^{+-})/(I^{++} + I^{+-})$, where I^{++} and I^{+-} are the PL intensity for co- and cross-polarizations of the excitation and detection, respectively. The PL polarization was recorded at the photon energy corresponding to the maximum of the PL band of the sample. Some experiments have been performed using different helicities of optical excitation and the PL detection in a fixed helicity.

To study the dynamics of nuclear polarization, we used an amplitude modulation of laser beam using an acousto-optic modulator to produce pulses with various bright and dark time durations. The spin polarization of the resident electrons was monitored through the effect of negative circular polarization (NCP), $\rho < 0$, of the PL observed for singly charged QDs. The mechanism of NCP of the PL of QDs has been extensively discussed in Refs. [29–31], where it was shown that the presence of NCP is the result of optical orientation of the resident electrons. The amplitude of NCP is proportional to the projection of electron spin onto the optical axis z, averaged over the QD ensemble [21]

$$A_{\mathrm{NCP}} \sim 2S_z. \tag{1}$$

The amplitude of the PL polarization, A_{NCP}, increased with rising excitation power at relatively low excitation levels (see Fig. 1). A further rise of the power resulted in saturation of the A_{NCP}, which indicates a high level of electron spin polarization. The pump powers used in our experiments were sufficiently high to totally polarize the electron spin.

3 Dynamics of Nuclear Polarization in a Transverse Magnetic Field [26]

Dynamics of nuclear polarization in QDs in the magnetic field perpendicular to the optical axis (in the Voigt geometry), until recently, were not actually investigated. An application of the transverse magnetic field reduces the degree of circular polarization of photoluminescence from semiconductors (the Hanle effect). This is

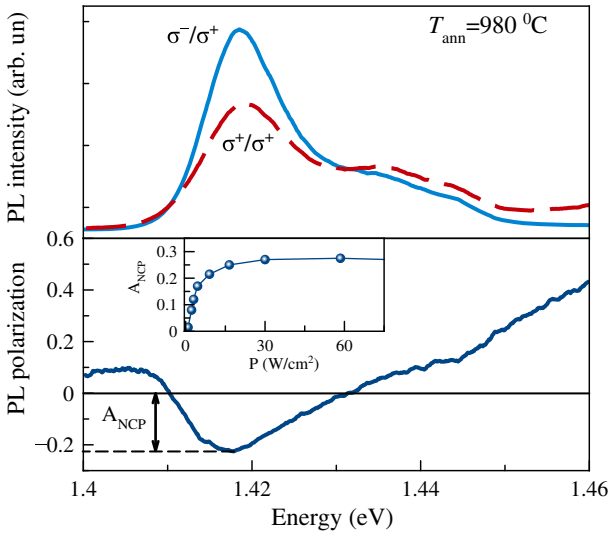

Fig. 1 Typical PL spectra (*top curves*) measured at $\sigma+$ excitation and co- and cross-polarized detection and the degree of circular polarization (*bottom curve*) for sample annealed at 980 °C. The definition of amplitude of the negative circular polarization is illustrated by the *arrow* marked A_{NCP}. *Inset* shows the power dependence of A_{NCP}

the effect of electron (or exciton) spins precession about the magnetic field. The shape of Hanle curve can be changed by effective magnetic field of nuclear polarization [18, 32]. This makes it possible to study the dynamics of nuclear polarization experimentally measuring the Hanle effect in the kinetic regime, i.e., with time resolution.

The first observations of the time-resolved Hanle effect in an ensemble of negatively charged (In,Ga)As/GaAs QDs [33] demonstrated that experiments of this kind would provide an effective tool for examining the dynamics of a nuclear spin system. In this section we discuss systematic experimental data used for studying the nuclear polarization buildup and decay times for the structure annealed at 900 °C (sample A). In these experiments, the amplitude modulation of optical pumping with various dark and excitation times, t_d and t_{exc}, has been used.

The Hanle curves obtained under strong pumping for the sample under study are similar in shape to those observed previously for donor-bound electrons, in qualitative agreement with predictions of a classical model of DNP in a transverse magnetic field [7, 8]. However, the classical model fails to explain an increase in the Hanle curve width with the optical pumping intensity, which was observed in these experiments. Following [33, 34], one can suppose that the Hanle curve broadening is due to nuclear polarization stabilized by quadrupole splitting of nuclear spin states. An analysis of time-resolved measurement data provides quantitative estimates of the rise and decay times for longitudinal and transverse nuclear fields in the structures under study. To examine the nuclear polarization buildup, the NCP was measured as a function of time after when the pump pulse had arrived, using the multichannel photon counting system.

Nuclear spin relaxation was examined by detecting photoluminescence during a short interval, $t_{det} = 1$ ms, at the start of pumping after various dark times. The pumping was supposed to have a weak effect on nuclear polarization during the detection time. The degree of polarization was measured as a function of dark time by varying t_d from 20 μs to 50 ms. Figure 2a shows the Hanle curves obtained for several dark times, and Fig. 2b shows the central part of the curves. It is clear that the curves corresponding to the short dark times are similar to that obtained under CW pumping. In particular, a pronounced W-profile is observed, and the curves are wide. An increase of the dark time smooths out the W-profile and diminishes the width of the Hanle curve.

The observed modifications of Hanle curves suggest that the development of nuclear polarization generally leads to a decrease in electron spin polarization in weak transverse magnetic fields and its increase in strong fields. It is obvious that these effects are associated with two different processes, namely with the dynamics of the longitudinal and transverse components of nuclear field. The dynamics of the longitudinal component, $B_{DNP||}$, of nuclear field can be inferred from the time evolution of the dips around the central peak.

Information about the behavior of the transverse component, $B_{DNP\perp}$, of nuclear field can be extracted from analysis of the width of the Hanle curve. Its large width has been attributed to the formation of $B_{DNP\perp}$ stabilized by quadrupole splitting of nuclear spin states along the optical axis [34]. Since the longitudinal component $B_{DNP||}$ plays no significant role in strong applied magnetic fields [7, 8], dynamics of

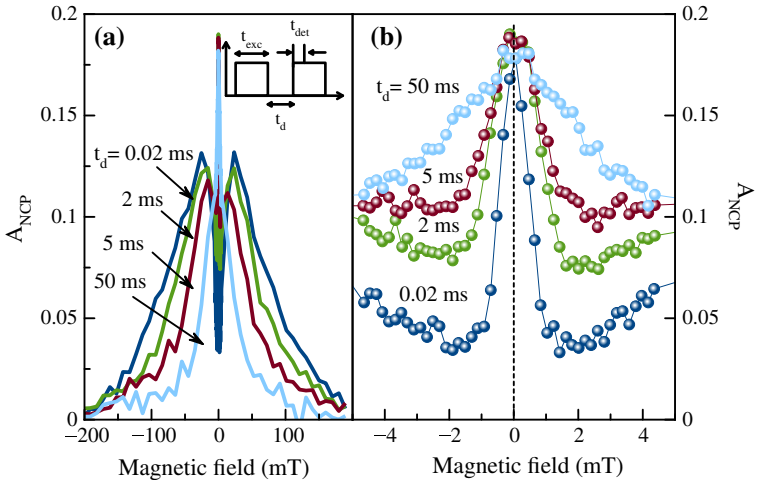

Fig. 2 Hanle curves at the fixed excitation time $t_{exc} = 100$ ms, and varied dark time t_d: **a** the complete curves; **b** the central part of the curves

$B_{DNP\|}$ and $B_{DNP\perp}$ can be inferred separately from behavior of electron spin polarization in weak and strong fields, respectively. Accordingly, to analyze experimental data, a model is required that relates the degree of electron spin polarization to the magnitudes of the corresponding DNP components.

The measured degree of PL polarization is proportional to the electron spin projection on the direction of observation:

$$S_z = S\cos\vartheta^2 = S\frac{B_{tot,z}^2}{B_{tot}^2}. \tag{2}$$

Here S quantifies the degree of optically induced electron spin orientation and ϑ is the angle between the direction of observation (the optical axis) and the total field, $B_{tot} = B + B_N$, which is the sum of the applied field B and the nuclear field, $B_N = B_f + B_{DNP}$, including the effective nuclear spin fluctuation, B_f, generated by the randomly oriented nuclear spins [2]. Since the electron spin in QD interacts with the limited number of nuclear spins, the fluctuation field B_f is significantly larger than that for the donor-bound electron spins in a bulk material and achieves several tens of milliteslas [35]. Therefore, we can evaluate only an ensemble averaged spin.

The degree of electron spin polarization can be represented by the general expression

$$\rho = S_z/S = \frac{\left(B_{DNP\perp}^2 + 0.5B_{f\perp}^2\right)}{\left(B + B_{DNP\|}\right)^2 + B_{DNP\perp}^2 + \langle B_f^2\rangle}, \tag{3}$$

where $\langle B_f^2\rangle = \langle B_{f\|}^2\rangle + B_{f\perp}^2 = 3\langle B_{f\|}^2\rangle$. The last relation holds when the dynamic nuclear polarization is insignificant and the nuclear spin fluctuations are statistically isotropic.

Experimental data can be analyzed by the use of Eq. (3) in two special cases of particular importance. According to [7], the longitudinal component $B_{\mathrm{DNP}\|}$ of nuclear field appears only in the W-profile region of the Hanle curve, where the applied field is negligible compared to the nuclear spin fluctuation field [2, 36]. Then, it holds for this region that

$$\rho \approx \frac{\left(B_{\mathrm{DNP}\perp}^2 + 0.5B_{\mathrm{f}\perp}^2\right)}{\left(B_{\mathrm{DNP}\|}\right)^2 + B_{\mathrm{DNP}\perp}^2 + 3\langle B_{\mathrm{f}\|}^2\rangle} \tag{4}$$

In the other limit of the strong applied magnetic fields (when $B \gg B_{\mathrm{DNP}\|}$), the degree of polarization is described as:

$$\rho \approx \frac{\left(B_{\mathrm{DNP}\perp}^2 + 0.5B_{\mathrm{f}\perp}^2\right)}{B^2 + B_{\mathrm{DNP}\perp}^2 + 3\langle B_{\mathrm{f}\|}^2\rangle} \tag{5}$$

Thus, the time dependence of ρ can be examined in the strong and weak magnetic fields that allow one to determine respective kinetics of the longitudinal and transverse components of nuclear polarization.

The analysis of time-dependent nuclear polarization is based on the assumption that the growth of each component of the nuclear polarization after the start of pumping and its decay during the dark time can be described by expressions, $y = B_{\mathrm{DNP}}^0[1 - \exp(-t/\tau)]$ and $y = B_{\mathrm{DNP}}^0 \exp(-t/\tau)$, where τ is a characteristic time of the buildup or decay of the nuclear polarization, respectively. For the weak magnetic field, the numerator and denominator in Eq. (4) can be divided by $< B_{\mathrm{f}\|}^2 >$ and parameters a and b can be introduced,

$$a^2 = \frac{\left(B_{\mathrm{DNP}\perp}^0\right)^2}{\langle B_{\mathrm{f}\|}^2\rangle}, \quad c^2 = \frac{\left(B_{\mathrm{DNP}\|}^0\right)^2}{\langle B_{\mathrm{f}\|}^2\rangle},$$

to find respective expressions describing the rise and decay of the longitudinal component of nuclear polarization:

$$\rho \approx \frac{0.5a^2 + 1}{c^2\left(1 - \mathrm{e}^{-t/\tau}\right)^2 + a^2 + 3}, \tag{6}$$

$$\rho \approx \frac{0.5a^2 + 1}{c^2\mathrm{e}^{-2t/\tau} + a^2 + 3}. \tag{6'}$$

For the case of strong applied magnetic fields, respective Eq. (5) can be rewritten in a similar way to describe the rise and decay of the transverse component of nuclear polarization, respectively.

$$\rho \approx \frac{0.5\left(1 - \mathrm{e}^{-t/\tau}\right)^2 + c'^2}{a'^2 + \left(1 - \mathrm{e}^{-t/\tau}\right)^2 + 3c'^2}, \tag{7}$$

$$\rho \approx \frac{0.5\mathrm{e}^{-2t/\tau} + c'^2}{a'^2 + \mathrm{e}^{-2t/\tau} + 3c'^2}, \tag{7'}$$

where $a'^2 = \frac{B^2}{\left(B_{\mathrm{DNP}\perp}^0\right)^2}$, $c'^2 = \frac{\langle B_{\mathrm{f}\|}^2\rangle}{\left(B_{\mathrm{DNP}\perp}^0\right)^2}$.

Figures 3 and 4 show results of the analysis of temporal dependences of the PL polarization measured for different points of the Hanle curves after the start of optical pumping. These data have been obtained from experimental data measured at the long fixed dark time. The values of ρ are refined to take into account a partial depolarization of the PL because of contributions from neutral QDs. Experimental data were processed to determine the time-resolved degrees of polarization corresponding to different applied magnetic field strengths. Figure 4 demonstrates a

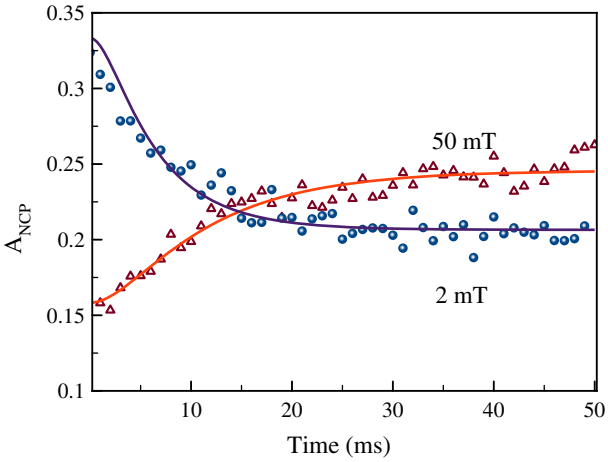

Fig. 3 Example of the time-dependent degree of PL polarization measured at different magnetic fields. Zero time corresponds to the start of optical pumping after long dark time when the nuclear polarization has totally relaxed. *Symbols* represent experimental results; *solid curves* are approximations by Eqs. (6) and (7)

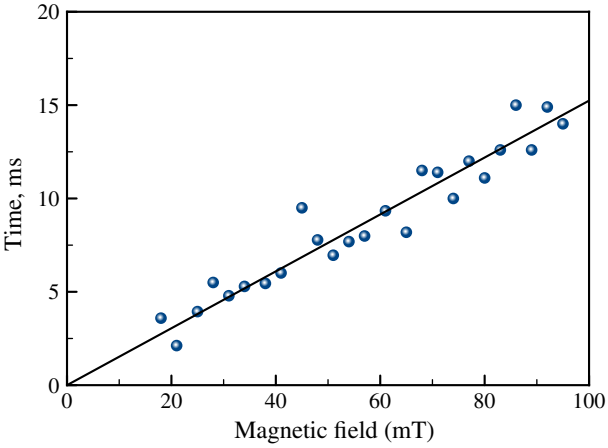

Fig. 4 Magnetic field dependence of the buildup time of the transverse DNP field component. Points are taken from analysis of the experimental data. The *solid curves* are drawn for clarity

large difference between kinetics of the polarization degree for the weak and strong magnetic field conditions (a few mT and higher than 20 mT, respectively).

At $B = 2$ mT (the lowest point of a dip in the W-structure of Hanle curves) where nuclear field $B_{\mathrm{DNP}\|}$ plays the dominant role, the degree of polarization decreases with time elapsed (Fig. 4), signifying an increase in $B_{\mathrm{DNP}\|}$. This time dependence of ρ determined from experimental data can be fitted by Eq. (6) only when one assumes that the transverse component of nuclear field is sufficiently weak, $B^2_{\mathrm{DNP}\perp} \ll \langle B^2_{\mathrm{f}\|} \rangle$, i.e., $a^2 \ll 1$. This approximation gives rise to the characteristic rise time for $B_{\mathrm{DNP}\|}$, $\tau_\| \approx 6$ ms.

In the large magnetic fields when the transverse nuclear field plays the main role, the experimentally determined growth of the PL polarization with time is well fitted by Eq. (7), see respective curve in Fig. 3. An analysis shows that all the temporal dependences of the PL polarization rise measured for $B > 20$ mT can be well fitted by this function. The characteristic rise time obtained from the fitting linearly depends on the external magnetic field as it shown in Fig. 4. As it is seen, the time increases from approximately 2.5–15 ms with an applied magnetic field varied from 20 to 100 mT.

Similar procedure can be used to analyze the Hanle curve profiles measured after different dark times, see Fig. 5. The experimental results were converted into spin polarization kinetics for several values of applied magnetic field strength (as in Fig. 4) and the resulting curves were fitted by Eqs. (6′) and (7′). The curves in Fig. 5 are examples of such fits. The fitting parameters were used to evaluate the initial longitudinal and transverse nuclear fields, as well as the corresponding decay times. The decay time of the longitudinal component, $B_{\mathrm{DNP}\|}$, calculated using the experimental data for $B = 2$ mT is found to be $\tau \approx 5.5$ ms, which is close to the corresponding rise time reported above.

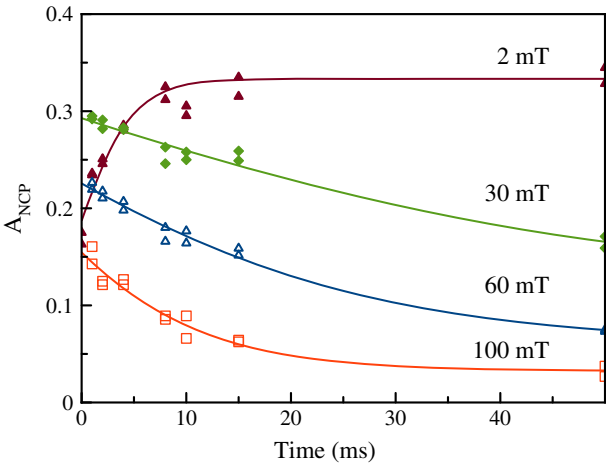

Fig. 5 Kinetics of polarization degree obtained at different magnetic fields by the analysis of experimental results for various dark times. *Symbols* represent experimental data; solid curves are approximations by Eqs. (6′) and (7′)

However, the decay time of the transverse component of nuclear polarization, $B_{\mathrm{DNP}\perp}$, differs significantly from its rise time. Moreover, its time variation in an applied magnetic field exhibits an opposite trend, whereas the rise time increases with the magnetic field (Fig. 4), the decay time rapidly decreases (Fig. 6). Accordingly, these times are approximately equal in strong magnetic fields but differ by a factor of several tens at $B = 20$ mT.

An analysis shows that the longitudinal and transverse components of nuclear polarization in the QDs under study exhibit widely different dynamical patterns. The behavior of longitudinal polarization is relatively simple. After the start of optical pumping, this component increases with a characteristic time of approximately 6 ms to a limit magnitude corresponding to an effective nuclear field of 30–40 mT. After the end of pumping, the longitudinal component decays over a similar time scale.

The behavior of the component of dynamic nuclear polarization perpendicular to the applied magnetic field is much more complicated. Up to now there is no straightforward explanation of so large difference in behavior of the rise and decay times, their opposite variations with applied magnetic field, and the increase in magnitude of this component with the magnetic field. One can assume that these effects indicate that the dominant contributions to the buildup of longitudinal and transverse polarization components come from states with different spin projections on the direction of observation.

Summarizing this section, we should note that an experimental study of the time-dependent circular polarization of PL from a QD ensemble as a function of magnetic field applied perpendicular to the optical axis (the time-resolved Hanle effect) allows one to study temporal evolution of the dynamic nuclear polarization. For the QDs characterized by strong quadrupole splitting of nuclear spin states, the experimental data can be analyzed on the base of separate treatment of the

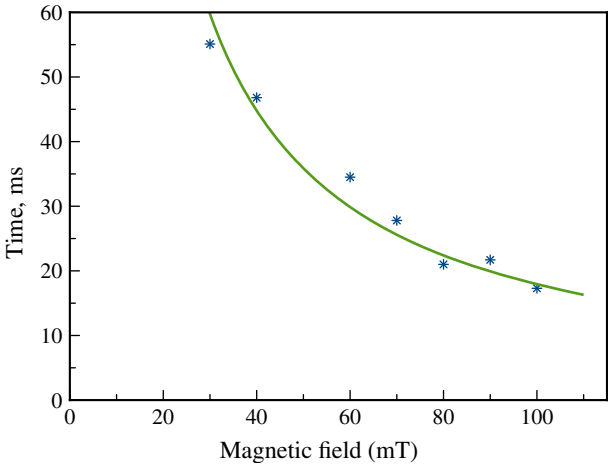

Fig. 6 Magnetic field dependence of the decay time of the transverse DNP-field, $B_{\mathrm{DNP}\perp}$. *Symbols* are taken from analysis of the experimental data. The *solid curves* are drawn for clarity

longitudinal and transverse components of the nuclear spin polarization. The phenomenological model discussed here takes into account the contribution of nuclear spin fluctuations, which were ignored in many previous studies of Hanle curves. The model is validated both by the fact that the fluctuating field is independent of applied magnetic field and by good quantitative agreement with results of other studies [16, 35]. Exploiting this model, important information about the rise and decay times of each component of nuclear polarization in QDs in a transverse magnetic field is obtained. The rise and decay times of the component parallel to the applied field were found to be almost equal (approximately 5 ms) for discussed QDs. However, the dynamics of the transverse component is much more complicated: the corresponding rise and decay times strongly differ and have opposite dependence on the magnetic field strength. Furthermore, the magnitude of the transverse component created by continuous wave pumping significantly increases with applied magnetic field. This unexpected behavior of nuclear spin polarization can be attributed to the nuclear spin relaxation via interaction with photoexcited carriers.

4 Role of Nuclear Spin Fluctuations [27]

The effect of the nuclear spin fluctuations (NSF) in the (In,Ga)As/GaAs QDs can be studied in more detail by means of the careful measurements and analysis of the Hanle curves in the weak magnetic fields (0–20 mT), where the NSF effect is expected to be the strongest. In this section, the Hanle curves measured under optical excitation of moderate intensity and at different strengths of an additional magnetic field applied along the optical axis (the longitudinal magnetic field) will be discussed. The representative set of the experimentally measured Hanle curves for the sample B annealed at temperature 980 °C is shown in Fig. 7. These curves are compared with theoretical results obtained in the framework of two models. One model includes the NSF and another one takes into account only the mean Overhauser fields [25]. In both the models, the mean Overhauser field has been calculated within the spin temperature approach. The analysis shows that the mean-field model fails to describe the features of the Hanle curve around zero transverse magnetic field, where the W-structure appears, in a certain range of longitudinal magnetic fields B_z. The model including NSF, on the other hand, yields good fits of the experimental data, with a reasonable choice of parameters, for all experimental conditions except for the exact compensation of the Knight field with B_z. In the latter case, the nuclear quadrupole effects caused by the strain in the QDs probably play the dominant role.

The Hanle curves measured when a small longitudinal magnetic field is applied are compared with the dependences calculated in the framework of the nuclear spin cooling model. For positive B_z, which, for the helicity of excitation used in the experiments, is codirected to the Knight field, the experimental and calculated curves are found to be in qualitative agreement with each other. The analysis shows that the effective nuclear field in this case is codirected to the external magnetic field and thus "amplifies" it. This amplification results in a gradual decrease of spin

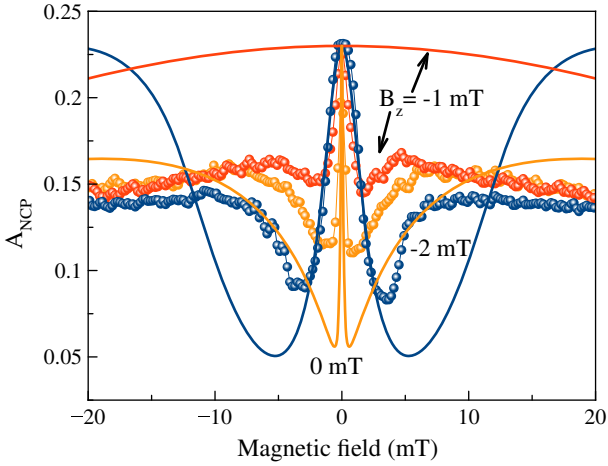

Fig. 7 Comparison of Hanle curves calculated in the framework of standard cooling model (*solid lines*) with the experimental data (points) for negative longitudinal external fields B_z

polarization and, correspondingly, of PL polarization beyond the central peak with rising B_z.

When B_z is negative, the effective field is antiparallel to the Knight field. When $B_z = -B_e$, the compensation of the longitudinal component of total field occurs. According to Refs [7, 18], the nuclear spin cooling is not possible in this case. This should result in the disappearance of the W-structure, as it is shown in Fig. 7 for the Hanle curve calculated for $B_z = -1$ mT. At more negative B_z, the W-structure appears again, but the additional maxima run away from the central peak with increasing $|B_z|$, maintaining the same amplitude as that of the central peak, see the curve in Fig. 7 calculated for $B_z = -2$ mT. This behavior of the calculated Hanle curves is explained by the fact that in this case the nuclear field is directed against the total effective magnetic field affecting the nuclei. The x component of the nuclear field, B_{Nx}, is compensated by the transverse magnetic field B_x at some magnitude of B_x that gives rise to the appearance of the additional maxima.

These numerical results, however, are in strong contradiction with the experimental observations as it is seen in Fig. 7. In the experiment, the central peak of the measured Hanle curves is always higher than the other parts of the Hanle curve at any negative B_z. We want to stress that this disagreement between the theory and the experiment cannot be eliminated for any values of the adjustable parameters. Therefore, this contradiction is of principal importance and indicates that the model of the mean nuclear field ignores some mechanism causing depolarization of the electron spin at nonzero transverse magnetic field, including the points where it is totally compensated by the nuclear field. In the cooling model, such mechanisms are not provided; therefore, this model is not able to describe the experimental data.

To extend the standard cooling model, one should take into account that the effective nuclear field consists of a regular component, B_N, created by the nuclear

spin polarization, and a fluctuating component, B_f, appearing due to the random orientation of the limited number of nuclear spins interacting with the electron spin [37]. The estimates given in Refs. [19, 38] for similar QDs show that the average magnitude of the fluctuating nuclear field is of the order of tens of milliTesla.

In the absence of the dynamic nuclear polarization, the dependence of the average electron spin polarization on the transverse external magnetic field within this approximation is a bell-like curve, which can be well fitted by a Lorentzian:

$$\rho(B) \approx \frac{\langle B_{\mathrm{f}z}^2 \rangle}{B^2 + \langle B_\mathrm{f}^2 \rangle} \tag{8}$$

Here $\langle B_\mathrm{f}^2 \rangle = \langle B_{\mathrm{f}x}^2 \rangle + \langle B_{\mathrm{f}y}^2 \rangle + \langle B_{\mathrm{f}z}^2 \rangle$, where $\langle B_{\mathrm{f}\alpha}^2 \rangle$ is the squared α component ($\alpha = x, y, z$) of the NSF averaged over the QD ensemble.

When the regular nuclear field B_N with nonzero components $B_{\mathrm{N}x}$ and $B_{\mathrm{N}z}$ is created by the dynamic polarization of nuclei, a generalization of Eq. (8) is required. In addition, in the experiments discussed here, the external magnetic field has not only the transverse component but also some longitudinal one. For this case a simple vector model [27] allows one to write down the following expressions for the z and x components of the averaged electron spin $\mathbf{S}$:

$$S_z = S_0 \frac{(B_z + B_{\mathrm{N}z})^2 + \langle B_{\mathrm{f}z}^2 \rangle}{(B_x + B_{\mathrm{N}x})^2 + (B_z + B_{\mathrm{N}z})^2 + \langle B_\mathrm{f}^2 \rangle}, \tag{9}$$

$$S_x = S_0 \frac{(B_z + B_{\mathrm{N}z})(B_x + B_{\mathrm{N}x})}{(B_x + B_{\mathrm{N}x})^2 + (B_z + B_{\mathrm{N}z})^2 + \langle B_\mathrm{f}^2 \rangle}. \tag{9'}$$

Here S_0 is the initial (photocreated) electron spin polarization. It is assumed that the regular nuclear field $\mathbf{B}_\mathrm{N}$ is directed along the total effective field, $\mathbf{B}_\mathrm{tot}^{(\mathrm{N})}$, acting on the nuclei. It consists of the external magnetic field, $\mathbf{B} = \mathbf{B}_x + \mathbf{B}_z$, and of the Knight field, $B_e = b_e \mathbf{S} = b_e(\mathbf{S}_x + \mathbf{S}_z)$, created by hyperfine interaction with the electron spin. According to the standard cooling model, the nuclear field is described in the following way:

$$\boldsymbol{B}_\mathrm{N} = \boldsymbol{B}_\mathrm{tot}^{(\mathrm{N})} \frac{b'_\mathrm{N} \left(\boldsymbol{B}_\mathrm{tot}^{(\mathrm{N})} \cdot \boldsymbol{S}_\parallel \right)}{B_\mathrm{tot}^{(\mathrm{N})2} + \xi B_\mathrm{L}^2} \cdot \frac{4\boldsymbol{I}(\boldsymbol{I}+1)}{3} \tag{10}$$

We should stress that the nuclear polarization occurs due to deviation of the direction of the electron spin polarization (direction of vector $\mathbf{S}$) and the direction of the nuclear field $\mathbf{B}_\mathrm{N}$, which coincides with direction of $\mathbf{B}_\mathrm{tot}^{(\mathrm{N})}$. This is described by $b_\mathrm{N}(\mathbf{B}_\mathrm{tot}^{(\mathrm{N})} \cdot \mathbf{S})$ in the nominator of Eq. (10), where b'_N is the effective field of totally polarized nuclei affecting the electron spin.

The above equation allows one to obtain the following expressions for the x and z components of the nuclear field:

$$B_{\mathrm{N}x} = (B_x + b_e S_x) \frac{b_\mathrm{N} \left(B_z S_z + B_x S_x + b_e S_x^2 + b_e S_z^2 \right)}{(B_x + b_e S_x)^2 + (B_z + b_e S_z)^2 + \xi B_\mathrm{L}^2} \tag{10'}$$

$$B_{Nz} = (B_z + b_e S_z)\frac{b_N\left(B_z S_z + B_x S_x + b_e S_x^2 + b_e S_z^2\right)}{\left(B_x + b_e S_x\right)^2 + \left(B_z + b_e S_z\right)^2 + \xi B_L^2} \qquad (10'')$$

Numerical factor $4I(I+1)/3$ in Eq. (10) is included in parameter $b_N = b'_N 4I(I+1)/3$, which is considered as a fitting parameter. Coefficient b_e is given, in principle, by expression [1]: $b_e = -(16\pi/3)\mu_B \xi^2$, where μ_B is the Bohr magneton and ζ is the electron density on a nucleus. The negative sign means that the direction of the Knight field is opposite to that of the electron spin. Because the electron density is dependent on the QD size, which can sufficiently vary from dot to dot, the value of ζ is unknown a priori.

For modeling the Hanle curves, the whole system of Eqs. (9), (9′), (10′), and (10‘‘) is solved relative to unknown S_z and their real roots are used. Examples of the calculated Hanle curves are shown in Fig. 9. As seen, reasonable agreement between calculated and measured curves is observed for negative B_z. Some deviations from the experiment occur for magnetic fields B_z in the range from −0.5 to −1 mT, where the theoretically calculated amplitude of the central peak is considerably smaller than the one observed experimentally (see inset in Fig. 8). The strong decrease of the peak amplitude obtained in the calculations is due to the depolarization of the electron spin by the nuclear spin fluctuations, when the longitudinal component of total field disappears and the nuclear field does not build up. Experiments also show the decrease in the central peak of about 20%, which is, however, significantly smaller than the one predicted theoretically. A possible reason for this discrepancy between the theory and the experiment could be related to the spread of Knight fields in the QD ensemble, which is ignored in the theory. Another possible reason is the polarization of quadrupole-split nuclear spin states, which can stabilize the electron spin polarization [34]. Further study is needed to clarify this problem.

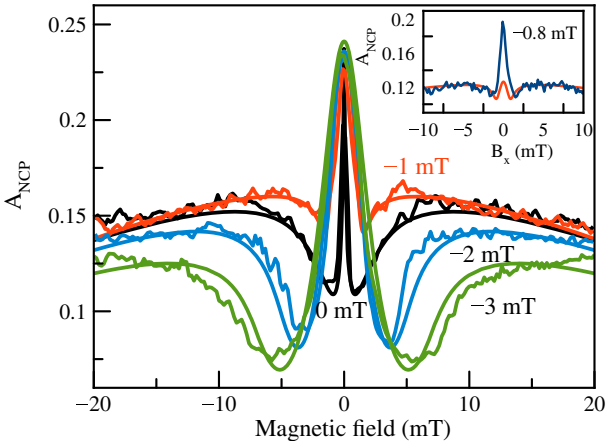

Fig. 8 Experimentally measured curves (*noisy lines*) and results of calculations by taking into account the NSF (*smooth solid lines*) for negative longitudinal external fields B_z

The results of the calculations point out that the effect of nuclear spin fluctuations is indeed important for the QDs under study. The good agreement between theory and experiment for the whole range of B_z (with the only exception mentioned above) allows one to consider the physical meaning of the parameters obtained from the fitting and their dependence on the longitudinal magnetic field. In particular, the NSF amplitude, $\sqrt{B_{fz}^2}$, can be chosen close to 25 mT for all the Hanle curves measured at various longitudinal magnetic fields. The good overall correspondence of the simulated and measured Hanle curves confirms the validity of the model developed.

The analysis of experimental data has confirmed the prediction of Ref. [2] about the significant effect of the nuclear spin fluctuations on the electron spin orientation due to strong localization of the electron in QDs. The observed behavior is considerably different from that in bulk semiconductor solid solutions studied in many works [7], in which the electron density is spread out over a huge number of nuclei and the effect of the NSF, as a rule, is negligibly small. The analysis allows one to evaluate the maximal value of the effective field of nuclear polarization created by optical pumping in the studied QDs to be about 200 mT. The effective field acting on the nuclei from the electron spin (the Knight field) in the sample under study is of about 1 mT when the electron spin is almost totally polarized.

5 Resonant Nuclear Spin Pumping [22, 28]

In this section we discuss the effect of resonant optical pumping of nuclear spin polarization in an ensemble of singly charged (In,Ga)As/GaAs QDs for sample B subjected to a transverse magnetic field. The electron spin orientation by the circularly polarized light is modulated at the frequencies of the nuclear magnetic resonances. It is found that a significant nuclear spin polarization, precessing about the magnetic field is created at such optical excitation.

An efficient technique to reach significant nuclear spin polarization (NSP) is optical pumping [7]. A relatively strong nuclear polarization (tens of percent) can be created by optical pumping of QDs in a magnetic field parallel to the optical axis (longitudinal field) [4–6]. Optical pumping is able to create a dynamic nuclear polarization also in a transverse magnetic field [18, 32]. It is commonly accepted [1] that the nuclear polarization is directed along the external magnetic field. The appearance of this longitudinal component corresponds to a difference in population of nuclear Zeeman sublevels and, therefore, is usually treated in terms of "nuclear spin cooling."

It has been experimentally demonstrated [22, 28] that not only the longitudinal but also the transverse NSP components of remarkable magnitude can be created in QDs. This effect is observed at the polarization-modulated optical excitation of singly charged (In,Ga)As/GaAs QDs, which results in a strong change of the dependence of PL polarization on a transverse magnetic field (Hanle curve), in particular, in the appearance of resonant features at the curves. The resonances are found to be related to spin transitions of the gallium, indium, and arsenic nuclei, which are influenced by magnetic field and quadrupole interaction. The observed

effect is a clear indication of a phasing of the nuclear spin states that corresponds to the creation of transverse NSP components precessing about the external magnetic field.

Figure 9 shows the magnetic field dependence of the NCP amplitude measured for different excitation protocols. All the curves show a decrease of NCP (the Hanle effect) with increasing magnetic field. For continuous-wave (cw) excitation with fixed polarization helicity, the Hanle curve consists of a narrow central peak and broad shoulders, together forming the so-called W-structure [18]. The W-structure clearly indicates the NSP that has built up for these excitation conditions. When amplitude modulation (AM) with a small on/off time ratio is used, the Hanle curve has a Lorentzian shape. Switching on the polarization modulation (PM) in addition to the amplitude modulation ("AM + PM" protocol in the inset of Fig. 10) does not change noticeably the Hanle curves, meaning that the nuclear polarization does not develop under such excitation conditions and the Hanle curve is determined solely by electron spin dynamics. Therefore, the Hanle curve measured in that way is called as the electronic peak ("*e* peak").

The Hanle curve measured for the polarization modulation only [curve (3) in Fig. 9] shows two additional maxima at approximately $B = \pm 10$ mT. The appearance of such additional maxima is the main topic of discussion in this section. The position of these additional maxima strongly depends on the polarization modulation frequency (Fig. 10). In particular, the positions are shifted to higher magnetic fields with increasing modulation frequency as it seen in the figure.

To identify the resonances, which contribute to the Hanle curves, the nuclear spin splitting in a transverse magnetic field has been analyzed (Fig. 11). The calculations are made taking into account the quadrupole splitting of nuclear spin states caused by the strain-induced gradient of the crystal field as well as by the statistical

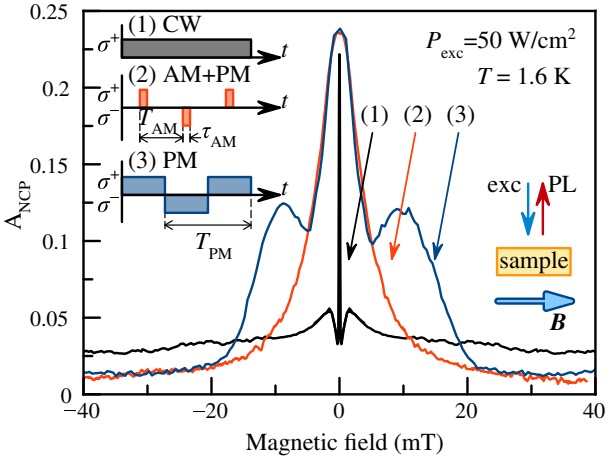

Fig. 9 Hanle curves measured for the cw optical excitation [*curve (1)*], for the modulated polarization of the excitation [$T_{PM} = 40$ μs, *curve (3)*], and for the polarization and amplitude modulation of the excitation [$T_{AM} = 20$ μs, $\tau_{AM} = 5$ μs, *curve (2)*]. The *top panels* sketch these different timing protocols

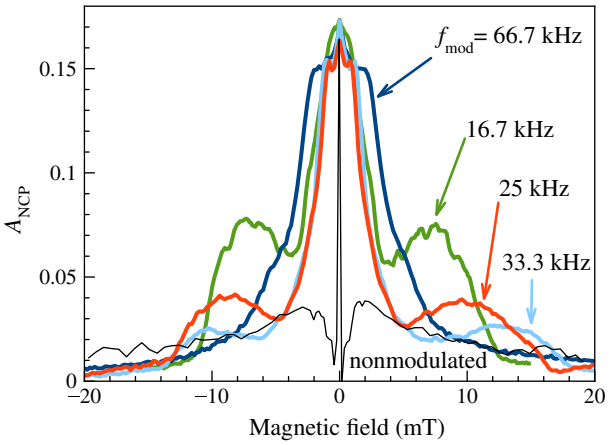

Fig. 10 Hanle curves measured for the excitation polarization modulated at different frequencies

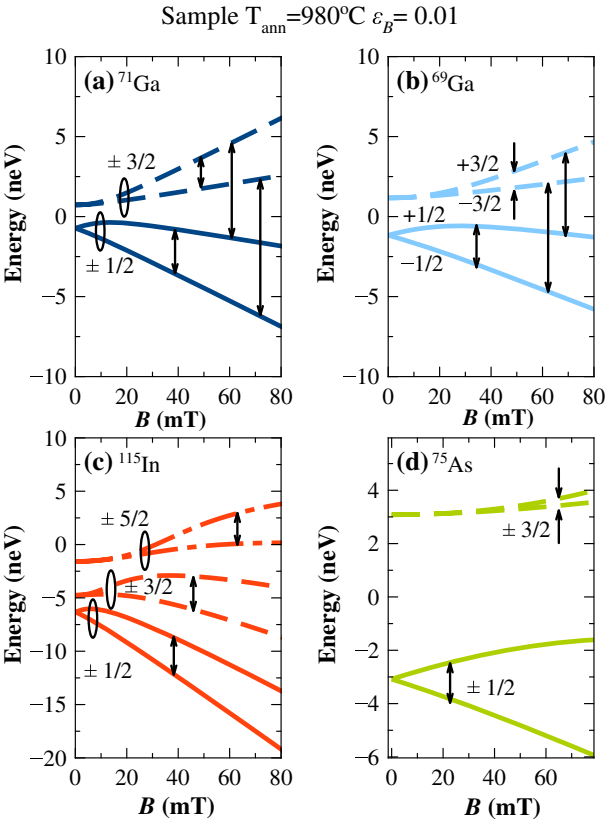

Fig. 11 Calculated energies of nuclear spin sublevels for isotopes ^{71}Ga, ^{69}Ga, ^{113}In, and ^{75}As as functions of magnetic field directed perpendicularly to the principal axis of the crystal field gradient tensor

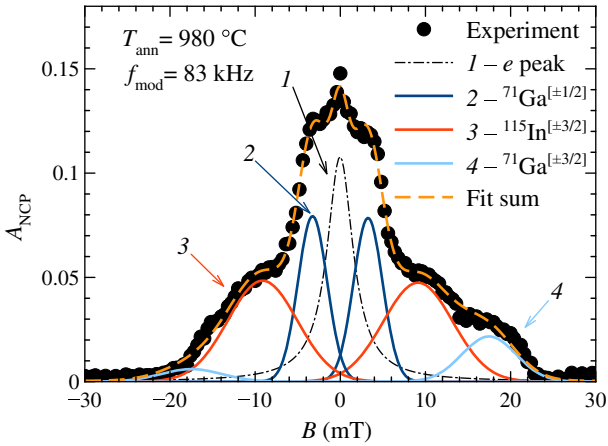

Fig. 12 Gaussian decomposition of Hanle curve measured for the sample annealed at 980 °C at the modulation frequency, $f_{PM} = 67$ kHz, in the presence of the radio frequency field (RFz field) [28]

population of crystal sites by Ga and In atoms. The QDs under study contain several types of nuclei (including isotopes): ^{69}Ga, ^{71}Ga, ^{75}As, ^{113}In, and ^{115}In. The principle axis of the strain-induced gradient is directed along the growth axis (z-axis).

In Fig. 11, the splitting of nuclear spin states by the magnetic field and the quadrupole interaction is calculated assuming a strain magnitude $\varepsilon_b = 0.01$ as it is estimated in [21] for sample annealed at $T = 980$ °C. Each resonance at a given energy determined by the modulation frequency is modeled by a Gaussian with amplitude and width as fit parameters. The analysis shows that the Hanle curves measured at different modulation frequencies can be well described using the calculated resonance energies.

The decomposition of a Hanle curve into a set of resonances is shown in Fig. 12. The central part of the curve is given by resonances $\langle +\frac{1}{2}| \leftrightarrow |-\frac{1}{2}\rangle$. The wide part of the Hanle curve can be well described by the resonances $\langle +\frac{3}{2}| \leftrightarrow |-\frac{3}{2}\rangle$ for the In and Ga nuclei, as well by the resonances $\langle +\frac{5}{2}| \leftrightarrow |-\frac{5}{2}\rangle$ for the In nuclei.

The comparison of the resonance positions obtained from the experiment with those obtained from the calculation of Zeeman splitting of nuclear spin states is shown in Fig. 13. Figure 13a demonstrates the data for transitions $+1/2 \leftrightarrow -1/2$, and Fig. 13b for the transitions $+3/2 \leftrightarrow -3/2, +5/2 \leftrightarrow -5/2$.

We should note here that the explanation of the Hanle curve peculiarities by peaks centered at certain resonance fields is not generally accepted, but rather the object of discussion. In [39], a peculiarity similar to the ones discussed here was considered as a peak. Furthermore, the authors of Refs. [6, 40, 41] observed experimentally the dispersion like peculiarities superimposed on a smooth Hanle curve. The key point for understanding the origin of the resonances discussed here is the appearance of a significant component of nuclear polarization in the plane perpendicular to the external magnetic field (the transverse component).

The creation of a transverse component is a resonant process, as the experiments show. For excitation with constant polarization of light, the polarized nuclear spins

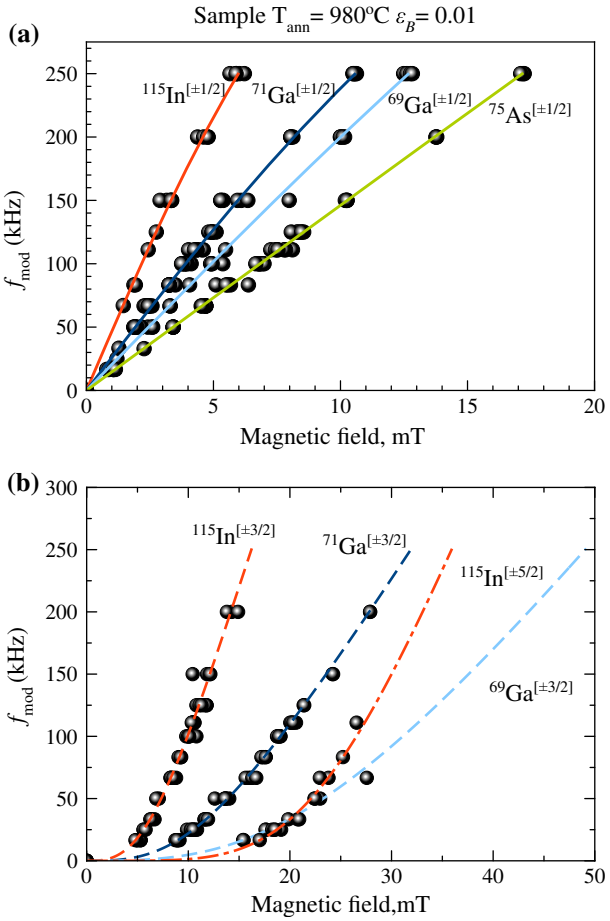

Fig. 13 Theoretically calculated frequencies of resonances as a function of magnetic field for nuclear spin states of the Ga, In, As nuclei in comparison with experimental data **a** for transitions $+1/2 \leftrightarrow -1/2$ and **b** for transitions $+3/2 \leftrightarrow -3/2$, $+5/2 \leftrightarrow -5/2$

are created with arbitrary phases so that a transverse component cannot be created. Only the resonant modulation of optical polarization results in the cophase pumping of a large number of nuclear spins, giving rise to resonant amplification of the transverse component of nuclear polarization.

In conclusion, we have discussed the experimentally observed significant nuclear polarization in the plane perpendicular to the external magnetic field in semiconductor QDs. The polarization is created by circularly polarized optical pumping modulated at a frequency that is resonant to one of the nuclear spin transitions. The effect, which may be termed the resonant optical pumping of nuclear spin polarization, is evidenced by several intense peaks in the Hanle curve. The number and amplitude of peaks considerably increase in the case of joint action of the polarization modulation of optical excitation and of the synchronous RF-field

application. In particular, the RF-field enhances the resonances related to transitions between the $|\pm 3/2>$ nuclear spin states split-off from the $|\pm 1/2>$ states by a quadrupole interaction.

Acknowledgements I thank I.V. Ignatev, R.V. Cherbunin, I.Ya. Gerlovin, K.V. Kavokin, S.Yu. Verbin and M.Yu. Petrov for fruitful discussions, D.R. Yakovlev and M. Bayer for collaboration, and D. Reuter and A. D. Wieck for the high-quality samples. The work is supported by the Russian Foundation for Basic Research (project no. 15-52-12020) and the Deutsche Forschungsgemeinschaft in the frame of International Collaborative Research Center TRR160.

References

1. M.I. Dyakonov (ed.), *Spin Physics in Semiconductors* (Springer Berlin Heidelberg, Berlin, 2008)
2. I.A. Merkulov, A.L. Efros, M. Rosen, Phys. Rev. B. **65**, 205309 (2002)
3. A.V. Khaetskii, D. Loss, L. Glazman, Phys. Rev. Lett. **88**, 186802 (2002)
4. D. Gammon, A.L. Efros, T.A. Kennedy, M. Rosen, D.S. Katzer, D. Park, S.W. Brown, V.L. Korenev, I.A. Merkulov, Phys. Rev. Lett. **86**, 5176 (2001)
5. P.-F. Braun, B. Urbaszek, T. Amand, X. Marie, O. Krebs, B. Eble, A. Lemaitre, P. Voisin, Phys. Rev. B **74**, 245306 (2006)
6. A.I. Tartakovskii, T. Wright, A. Russell, V.I. Fal'ko, A.B. Van'kov, J. Skiba-Szymanska, I. Drouzas, R.S. Kolodka, M.S. Skolnick, P.W. Fry, A. Tahraoui, H.-Y. Liu, M. Hopkinson, Phys. Rev. Lett. **98**, 026806 (2007)
7. V.G. Fleisher, I.A. Merkulov, in *Optical Orientation*, ed. by B.P. Zakharchenya, F. Meier (North-Holland, Amsterdam, 1984), Chap. 5, pp. 173–258
8. V.K. Kalevich, K.V. Kavokin, I.A. Merkulov, in *Spin Physics in Semiconductors*, ed. by M.I. Dyakonov (Springer-Verlag Berlin Heidelberg, Berlin, 2008), Chap. 11, p. 309
9. V.K. Kalevich, V.D. Kul'kov, V.G. Fleisher, JETP Lett. **35**(1), 20 (1982)
10. S.W. Brown, T.A. Kennedy, D. Gammon, E.S. Snow, Phys. Rev. B **54**, R17339(R) (1996)
11. D. Gammon, E.S. Snow, B.V. Shanabrook, D.S. Katzer, D. Park, Phys. Rev. Lett. **76**, 3005 (1996)
12. T. Belhadj, T. Kuroda, C.-M. Simon, T. Amand, T. Mano, K. Sakoda, N. Koguchi, X. Marie, B. Urbaszek, Phys. Rev. B **78**, 205325 (2008)
13. D. Gammon, S.W. Brown, E.S. Snow, T.A. Kennedy, D.S. Katzer, D. Park, Science **277**, 85 (1997)
14. P. Maletinsky, A. Badolato, A. Imamoglu, Phys. Rev. Lett. **99**, 056804 (2007)
15. E.A. Chekhovich, M.N. Makhonin, K.V. Kavokin, A.B. Krysa, M.S. Skolnick, A.I. Tartakovskii, Phys. Rev. Lett. **104**, 066804 (2010)
16. R.V. Cherbunin, S.Y. Verbin, T. Auer, D.R. Yakovlev, D. Reuter, A.D. Wieck, I.Y. Gerlovin, I.V. Ignatiev, D.V. Vishnevsky, M. Bayer, Phys. Rev. B **80**, 035326 (2009)
17. P. Maletinsky, C.W. Lai, A. Badolato, A. Imamoglu, Phys. Rev. B **75**, 035409 (2007)
18. D. Paget, G. Lampel, B. Sapoval, V.I. Safarov, Phys. Rev. B **15**, 5780 (1977)
19. B. Pal, Y. Masumoto, Phys. Rev. B **80**, 125334 (2009)
20. T. Auer, R. Oulton, A. Bauschulte, D.R. Yakovlev, M. Bayer, S.Y. Verbin, R.V. Cherbunin, D. Reuter, A.D. Wieck, Phys. Rev. B **80**, 205303 (2009)
21. K. Flisinski, I.Y. Gerlovin, I.V. Ignatiev, M.Y. Petrov, S.Y. Verbin, D.R. Yakovlev, D. Reuter, A.D. Wieck, M. Bayer, Phys. Rev. B **82**, 081308(R) (2010)
22. R.V. Cherbunin, K. Flisinski, I.Y. Gerlovin, I.V. Ignatiev, M.S. Kuznetsova, M.Y. Petrov, D.R. Yakovlev, D. Reuter, A.D. Wieck, M. Bayer, Phys. Rev. B **84**, 041304 (2011)
23. Y. Masumoto, K. Toshiyuki, T.S. Suzuki, M. Ikezawa, Phys. Rev. B **77**, 115331 (2008)
24. B. Urbaszek, X. Marie, T. Amand, O. Krebs, P. Voisin, P. Maletinsky, A. Högele, A. Imamoglu, Rev. Mod. Phys. **85**, 70 (2013)
25. A. Abragam, *The Principles of Nuclear Magnetism* (Clarendon Press, Oxford, 1961)
26. S.Y. Verbin, I.Y. Gerlovin, I.V. Ignatiev, M.S. Kuznetsova, R.V. Cherbunin, K. Flisinski, D.R. Yakovlev, M. Bayer, Zh. Eksp.Teor. Fiz. **141**, 778 (2012) [Sov. Phys. JETP **114**, 681 (2012)]
27. M.S. Kuznetsova, K. Flisinski, I.Y. Gerlovin, I.V. Ignatiev, K.V. Kavokin, S.Yu. Verbin, D.R. Yakovlev, D. Reuter, A.D. Wieck, M. Bayer, Phys. Rev. B **87**, 235320 (2013)

28. M.S. Kuznetsova, K. Flisinski, I.Y. Gerlovin, M.Y. Petrov, I.V. Ignatiev, S.Yu. Verbin, D.R. Yakovlev, D. Reuter, A.D. Wieck, M. Bayer, Phys. Rev B **89**, 125304 (2014)
29. S. Cortez, O. Krebs, S. Laurent, M. Senes, X. Marie, P. Voisin, R. Ferreira, G. Bastard, J.-M. Gérard, T. Amand, Phys. Rev. Lett. **89**, 207401 (2002)
30. I.V. Ignatiev, S.Y. Verbin, I.Y. Gerlovin, R.V. Cherbunin, Y. Masumoto, Opt. Spektrosk. **106**, 427 (2009) [Opt. Spectrosc. 106, 375 (2009)]
31. R.I. Dzhioev, B.P. Zakharchenya, V.L. Korenev, P.E. Pak, D.A. Vinokurov, O.V. Kovalenkov, I.S. Tarasov, Phys. Solid State **40**(9), 1587–1593 (1998)
32. O. Krebs, P. Maletinsky, T. Amand, B. Urbaszek, A. Lemaître, P. Voisin, X. Marie, A. Imamoglu, Phys. Rev. Lett. **104**, 056603 (2010)
33. R.V. Cherbunin, S.Y. Verbin, K. Flisinski, I.Y. Gerlovin, I.V. Ignatiev, D.V. Vishnevsky, D. Reuter, A.D. Wieck, D.R. Yakovlev, M. Bayer, J. Phys: Conf. Ser. **245**, 012055 (2010)
34. R.I. Dzhioev, V.L. Korenev, Phys. Rev. Lett. **99**, 037401 (2007)
35. M.Y. Petrov, G.G. Kozlov, I.V. Ignatiev, R.V. Cherbunin, D.R. Yakovlev, M. Bayer, Phys. Rev B **80**, 125318 (2009)
36. R.I. Dzhioev, V.L. Korenev, I.A. Merkulov, B.P. Zakharchenya, D. Gammon, A.L. Efros, D.S. Katzer, Phys. Rev. Lett. **88**, 256801 (2002)
37. I.A. Merkulov, G. Alvarez, D.R. Yakovlev, T.C. Schulthess, Phys. Rev. B **81**, 115107 (2010)
38. M. Ikezawa, B. Pal, Y. Masumoto, I.V. Ignatiev, S.Y. Verbin, I.Y. Gerlovin, Phys. Rev. B **72**, 153302 (2005)
39. Yu.G. Kusraev, E.S. Artemova, R.I. Dzhioev, B.P. Zakharchenya, I.A. Merkulov, V.G. Fleisher, Sov. Phys. Solid State **24**, 2705 (1982). **(in Russian)**
40. V.K. Kalevich, V.D. Kulkov, V.G. Fleisher, Fiz. Tverd. Tela (Leningrad) **22**, 1208 (1980) [Sov. Phys. Solid State **22**, 1208 (1980)]
41. M. Eickhoff, B. Lenzman, G. Flinn, D. Suter, Phys. Rev. B **65**, 125301 (2002)